Uniaxial ε-near-zero metamaterials for giant enhancement of the transverse magneto-optical Kerr effect

E. Moncada-Villa,[1] Osvaldo N. Oliveira, Jr.,[2] and J. R. Mejía-Salazar[3,*]

[1]*Escuela de Física, Universidad Pedagógica y Tecnológica de Colombia, Avenida Central del Norte 39-115, Tunja, Colombia*

[2]*Instituto de Física de São Carlos, Universidade de São Paulo, CP 369, 13560-970, São Carlos, SP, Brazil*

[3]*National Institute of Telecommunications (Inatel), 37540-000, Santa Rita do Sapucaí, MG, Brazil*

(Received 30 July 2020; revised 21 September 2020; accepted 22 September 2020; published 6 October 2020)

We demonstrate a giant enhancement of the transverse magneto-optical Kerr effect. In contrast to conventional magnetoplasmonic structures, we exploit surface plasmon resonances (SPRs) excited along the surface of a ferromagnetic substrate on which a uniaxial ε-near-zero (ENZ) metamaterial is grown. In this design, bulky prism couplers are not required and SPR sensors can be produced in integrated, miniaturized systems. We also obtained the analytical expression for the ENZ-SPR phase-matching condition, which can be used for the straightforward design of plasmonic and magnetoplasmonic devices.

DOI: 10.1103/PhysRevB.102.165304

I. INTRODUCTION

Magnetoplasmonics exploits strongly enhanced, highly confined electromagnetic fields (at plasmonic interfaces) to increase the magneto-optical (MO) activity of an adjacent MO surface [1–6] which may enable ultrafast magnetic storage [7–9], biosensing [10], optical filtering, and optical isolation devices [11–13]. Unfortunately, the effective transfer of these technologies from research laboratories to real-world applications can be hampered in conventional mechanisms for surface plasmon resonance (SPR) excitation. For instance, the need for a prism coupler for SPR excitation in Otto or Kretschmann configurations [14,15] precludes miniaturization and the development of integrated, portable devices. Integrable devices with giant enhancement of MO effects have been proposed with ε-near-zero (ENZ) materials, i.e., near-zero permittivity [16,17], but the fabrication of isotropic semiconducting oxide materials (operating near their plasma frequency) [18] can be costly and difficult to tune, being limited to the infrared ($\lambda > 1000$ nm). This demand for tunable, integrable magnetoplasmonic devices can be fulfilled with nanofabricated artificial materials with unique, unusual physical properties [19–22]. These manmade materials, commonly named metamaterials, can be divided into negative-refractive (or left-handed) materials [23,24], electric-negative materials [25], magnetic-negative materials [26,27], and hyperbolic metamaterials (HMMs) [28–31]. HMMs are advantageous compared to their counterparts in terms of fabrication and wavelength tuning because they are uniaxial anisotropic metamaterials in which one principal component of permittivity (ε) has opposite sign to the other two [29]. The permittivity tensor for these HMMs can be written as

$$\hat{\varepsilon} = \begin{pmatrix} \varepsilon_\perp & 0 & 0 \\ 0 & \varepsilon_\perp & 0 \\ 0 & 0 & \varepsilon_\parallel \end{pmatrix}, \tag{1}$$

where the components parallel and perpendicular to the anisotropy axis are indicated by the subscripts $\parallel$ and $\perp$, respectively. In analogy with semiconducting-based ENZ metamaterials, i.e., working near the plasma frequency, ENZ properties of HMMs have been investigated near the frequency where the corresponding negative permittivity-component changes its sign [28,31]. In general, there are two different regimes of interest. The first one is the ENZ-HMM, where the permittivity components are $\varepsilon_\perp > 0$, with a negative-ENZ for $\varepsilon_\parallel$. Second, $\varepsilon_\perp > 0$ with a positive-ENZ for $\varepsilon_\parallel$. In the latter case, the metamaterials are simply known as uniaxial anisotropic ENZ metamaterials [28]. The corresponding frequency for $\varepsilon_\parallel \approx 0$ can be easily tuned from the visible to the infrared by controlling geometrical parameters of the building components [28–31]. Although uniaxial ENZ metamaterials have been studied for filtering, polarization control, and imaging [28], their application for MO enhancement and/or SPR excitation remains unexplored.

In this paper, we analytically and numerically demonstrate that nanostructured uniaxial ENZ metamaterials over MO surfaces are suitable for tunable, highly integrable magnetoplasmonic platforms. More specifically, we studied the transverse MO Kerr effect (TMOKE) of a nanostructure built as an uniaxial anisotropic ENZ slab grown on a ferromagnetic substrate, as illustrated in Fig. 1(a). TMOKE is usually defined as [32,33]

$$\text{TMOKE} = \frac{R_{pp}(+\mathbf{M}) - R_{pp}(-\mathbf{M})}{R_{pp}(+\mathbf{M}) + R_{pp}(-\mathbf{M})}, \tag{2}$$

where R_{pp} is the reflectivity for obliquely ($\theta \neq 0$) incident p-polarized light. The signs $\pm$ in parentheses indicate that the magnetization points along the $\pm y$ axis, respectively. This

*jrmejia@inatel.br

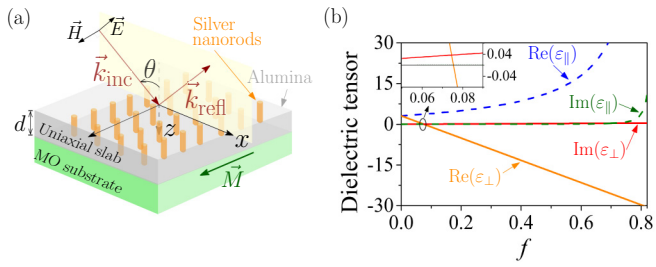

FIG. 1. (a) Pictorial description of an electromagnetic wave impinging on a uniaxial metamaterial slab, of thickness d, grown on a magneto-optical ferromagnetic substrate. The metamaterial is taken as made of metallic Ag nanorods immersed in a dielectric Al_2O_3 host. (b) Real and imaginary components, parallel and perpendicular, of the dielectric tensor of the metamaterial slab, as a function of the filling factor f of the metallic nanorods, for a working wavelength of 873 nm. The inset shows a zoom of the real and imaginary parts of $\varepsilon_\perp$ for $f = 0.075$.

effect is characterized by the relative change in the reflection amplitude of p-polarized light when the magnetization is reversed along the y axis. In contrast to conventional ferromagnetic materials [32], where TMOKE is typically of the order of 10^{-3}, we obtained amplitudes near 1.0 using our design. It is worth mentioning that this structure exhibits reduced losses in comparison with their semiconducting-based ENZ counterparts even for wavelengths in the visible [18]. Moreover, in contrast to previous proposals, the uniaxial ENZ working wavelength can be tuned from the visible to the infrared, enabling applications for integrated refractive index-sensing applications with commercial lasers.

II. THEORETICAL FRAMEWORK

Uniaxial metamaterials can be built with periodic arrangement of metallic nanowires embedded in a dielectric membrane [28] or by multilayers alternating metallic and dielectric films [30,31]. In both cases, the effective permittivity can be described using the effective medium theory [34]. In analogy to the experimental results in Ref. [28], we considered the uniaxial metamaterial slab made as an array of Ag nanowires with permittivity ε_r, embedded in an Al_2O_3 with permittivity ε_h, as depicted in Fig. 1(a). Therefore, we obtained the components of the permittivity tensor in Eq. (1) using

$$\varepsilon_\perp = \frac{\varepsilon_h(\varepsilon_h+\varepsilon_r)(1-f)+2f\varepsilon_r\varepsilon_h}{2f\varepsilon_h+(\varepsilon_r+\varepsilon_h)(1-f)}, \tag{3}$$

$$\varepsilon_\parallel = \varepsilon_h(1-f)+f\varepsilon_r, \tag{4}$$

where f is the filling factor, i.e., the volume fraction of metallic inclusions. Figure 1(b) shows the permittivity components of the uniaxial metamaterial as a function of f, with $\varepsilon_h = 3.092$ and $\varepsilon_r = -37.88 + 0.49i$, corresponding to the working wavelength $\lambda = 873$ nm.

The corresponding permittivity tensor for the MO substrate is described by [33]

$$\hat{\varepsilon}_{\rm MO} = \begin{pmatrix} \varepsilon & 0 & im\gamma \\ 0 & \varepsilon & 0 \\ -im\gamma & 0 & \varepsilon \end{pmatrix}, \tag{5}$$

where $m = \pm 1$ indicates the corresponding orientation of **M** along the y axis. Parameters in Eq. (5) are used as $\varepsilon_{\rm Fe} = -5.04 + 23.82i$ and $\gamma_{\rm Fe} = -1.52 - 0.04i$ [35], and $\varepsilon_{\rm Co} = -14.65 + 33.5i$ and $\gamma_{\rm Co} = 0.022 - 1.39i$ [36] for Fe and Co, respectively. The uniaxial ENZ behavior was tuned to $\varepsilon_\perp = 3.69067 + 0.00140304i$ and $\varepsilon_\parallel = 0.0183809 + 0.0369312i$, for $f = 0.075$, as indicated in the inset of Fig. 1(b).

Using the scattering matrix method [35,37], we calculated the corresponding reflectances $R_{\rm pp} = |r_{\rm pp}|^2$ from the uniaxial ENZ-MO structure in Fig. 1(a). Analytical expressions were obtained for $r_{\rm pp}$, as follows:

$$r_{pp} = \frac{(\beta_1-\beta_2)(\beta_2+\beta_3-k_x\eta_{3,xz})+e^{2iq_2d}(\beta_1+\beta_2)(\beta_2-\beta_3+k_x\eta_{3,xz})}{(\beta_1+\beta_2)(\beta_2+\beta_3-k_x\eta_{3,xz})+e^{2iq_2d}(\beta_1-\beta_2)(\beta_2-\beta_3+k_x\eta_{3,xz})}, \tag{6}$$

where $\beta_i = \eta_{i,xx}q_i$ $(i = 1,\ldots,3)$, with

$$k_x = \frac{\omega}{c}\sqrt{\varepsilon_1}\sin\theta, \tag{7}$$

$$q_1 = \frac{\omega}{c}\sqrt{\varepsilon_1}\cos\theta, \tag{8}$$

$$q_2 = \sqrt{\frac{\omega^2}{c^2}\frac{1}{\eta_{2,xx}} - \frac{\eta_{2,zz}}{\eta_{2,xx}}k_x^2}, \tag{9}$$

$$q_3 = \sqrt{\frac{\omega^2}{c^2}\frac{1}{\eta_{3,xx}} - k_x^2}, \tag{10}$$

$$\eta_{1,xx} = \varepsilon_1^{-1}, \tag{11}$$

$$\eta_{2,xx} = \varepsilon_\perp^{-1}, \tag{12}$$

$$\eta_{2,zz} = \varepsilon_\parallel^{-1}, \tag{13}$$

$$\eta_{3,xx} = \frac{\varepsilon}{\varepsilon^2-\gamma^2}, \tag{14}$$

$$\eta_{3,xz} = \frac{-im\gamma}{\varepsilon^2-\gamma^2}, \tag{15}$$

with the subscripts 1,2, and 3 indicating that the parameters are calculated for the incident medium, the uniaxial metamaterial, and the MO substrate, respectively, i.e., ε_1 corresponds to the permittivity for the incident medium.

III. RESULTS AND DISCUSSION

Rather than employing conventional magnetoplasmonic nanostructures with alternating noble metal (plasmonics) and ferromagnetic (MO) films, we used a uniaxial ENZ slab grown on a ferromagnetic substrate. SPRs are excited along the ENZ-MO interface through the ENZ-SPR phase-matching

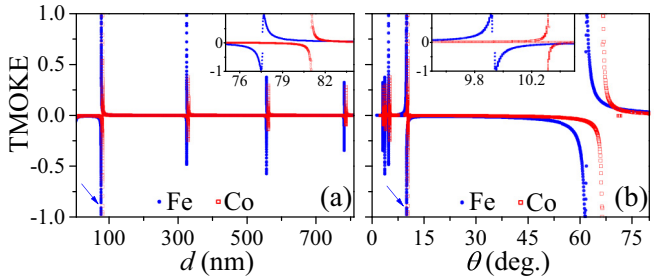

FIG. 2. TMOKE calculated as a function of $d \in [5\,\text{nm}, 810\,\text{nm}]$ and $\theta \in [0°, 80°]$. For easy identification of resonances, results are presented as functions of (a) d and (b) θ. Calculations were made using $\varepsilon_1 = 1.0$, i.e., considering the incident medium as air. The data in solid circles (blue color) were obtained with Fe as the substrate while the open squares (red color) refer to results for Co as substrate.

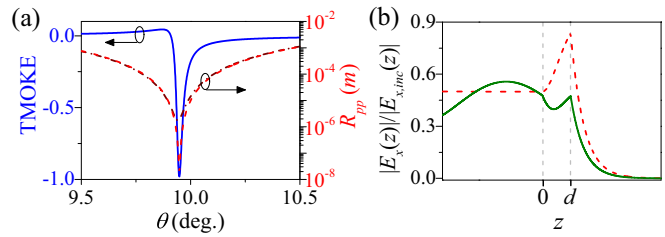

FIG. 3. (a) TMOKE (left-side scale) as a function of the incident angle is plotted by a solid line. The corresponding reflectance (right-side scale) for p-polarized light, with $m = +1$ ($m = -1$), is represented by a dashed (dash-dotted) line. (b) The electric field distribution along the structure for $\theta = 9.95°$ ($\theta = 15°$) is shown with a dashed (solid) line. Calculations were made for $d = 77.43$ nm on a Fe substrate.

condition, which we found from the condition of minimum reflectance as

$$\tan(q_2 d) = \frac{\beta_2^2 + \beta_1(\beta_3 - k_x \eta_{3,xz})}{\beta_2(\beta_1 + \beta_3 - k_x \eta_{3,xz})}. \tag{16}$$

This equation is not limited to the materials considered in this paper. On the contrary, it can be utilized to find the SPR condition of any uniaxial ENZ-based magnetoplasmonic structure with the ENZ metamaterial deposited on any ferromagnetic substrate. As the TMOKE resonances occur around the SPR condition, this latter equation can be used not only to describe the TMOKE peaks but also for a straightforward design of magnetoplasmonic structures. Previous theoretical and experimental studies about SPRs on Fe, Co, and Ni surfaces are primarily devoted to chemiluminescence emission and plasmonic fiber optic sensors [38,39], and the use for sensing in aqueous media is presented here.

Numerical calculations in Fig. 2 were carried out for substrates of Fe and Co for comparison purposes. Results were obtained varying simultaneously the slab thickness (d) of the uniaxial ENZ and the angle of light incidence (θ), in the ranges $d \in [5\,\text{nm}, 810\,\text{nm}]$ and $\theta \in [0°, 80°]$, for $\varepsilon_1 = 1.0$ (air). For visualization purposes, results are presented only as a function of d in Fig. 2(a) and only as a function of θ in Fig. 2(b). Higher losses in Co than in Fe at the working wavelength are responsible for the lower TMOKE peaks. To explain the TMOKE resonances in Fig. 2, we consider an uniaxial ENZ on a Fe substrate and ENZ slab thickness $d = 77.43$ nm under p-polarized light illumination with $\theta = 9.95°$, as indicated by arrows in Figs. 2(a) and 2(b). We expect a negative peak of maximum amplitude in TMOKE (~ -1), as observed from Fig. 3(a) (left-side scale). Reflectances (R_{pp}) are also shown in Fig. 3(a) (right-side scale) for $m = +1$ (dashed line) and $m = -1$ (dash-dotted line). The minimum in the reflectance spectra is due to the excitation of SPR at the ENZ-Fe interface.

The behavior for all the TMOKE resonances in Fig. 2 can be explained precisely with the analytical expression in Eq. (16). The SPR field enhancement at the uniaxial ENZ-Fe interface is also shown in Fig. 3(b), where the corresponding normalized E_x-field profile is plotted with dashed line for $m = +1$ with $d = 77.43$ nm and $\theta = 9.95°$, i.e., under the resonant condition. We also plotted in a solid line the E_x-field profile for the same d value but using $\theta = 15°$, corresponding to a negligible ($\sim 10^{-4}$) TMOKE value [see Fig. 2(b)] and a highly reflective behavior. Although the prototypical uniaxial-ENZ metamaterial has Ag nanorods in a matrix of Al_2O_3, our concept can be easily extended to other uniaxial metamaterials. In particular, experimentalists may employ techniques such as pulsed laser deposition to fabricate precise, highly tunable metallic nanorods embedded in an oxide matrix to obtain magnetoplasmonic platforms as proposed in this paper [40–42]. Some differences may appear between the theoretical model for the uniaxial metamaterial and their experimental responses due to small surface imperfections/variations [28], which we expect to be within the experimental tolerance. Figure 4 illustrates the possible application of the proposed structure for sensing based on changes of the refractive index in aqueous media. The incidence medium is taken as water with refractive index $n_1 = 1.335$ ($\varepsilon_1 = 1.78223$). Figure 4(a) shows TMOKE for the structure in Fig. 1(a) using $d = 77.43$ nm with a Fe substrate. Calculations were made for a refractive index of the incident medium varying from $n_1 = 1.335$ to $n_1 = 1.345$, in steps of $\Delta n_1 = 0.001$. The corresponding changes in the angle for the resonant TMOKE peak, associated with successive steps in the incident refractive index, are shown in

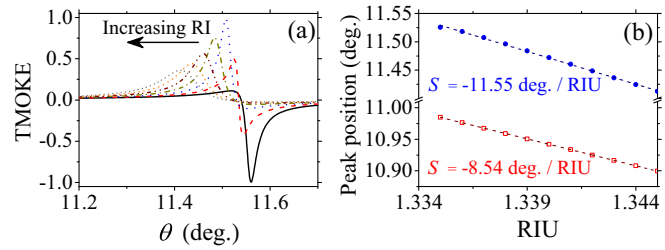

FIG. 4. (a) TMOKE as a function of the angle of incidence for different refractive indices of the incident medium for a Fe substrate. Calculations were made for a slab thickness $d = 77.43$ nm. The incident refractive index varied from 1.333 to 1.345 in steps of $\Delta n_1 = 0.001$. (b) TMOKE peaks as a function of the incidence angle and refractive index of the incident medium. Results are presented for substrates of Fe and Co with dashed lines with solid circles and open squares, respectively.

Fig. 4(b) by a dashed line with solid circles. The sensitivity is calculated here as $S = \frac{\partial \theta_{\text{peak}}}{\partial n_1}$, where θ_{peak} indicates the angle associated with a TMOKE peak for a specific value of n_1. As noted from Fig. 4(b), θ_{peak} changes linearly, thus the corresponding value of S can be obtained from a simple linear fitting. The detrimental effects from losses can be inferred by comparing with results for the same system but with Co as the substrate, shown in Fig. 4(b) by a dashed line with open squares. The sensitivity in these systems can be lower than their prism-based counterparts [43] but we expect that this seminal work may inspire further studies to circumvent this limitation for sensing. Moreover, the simplicity and high integrability of this concept can also lead to the development of magnetoplasmonic devices using other MO effects.

IV. CONCLUSIONS

In summary, we have shown that uniaxial ENZ metamaterials grown on ferromagnetic substrates can be used for highly integrable magnetoplasmonic platforms. Significantly, we found an analytical expression for the SPR condition in these structures, based on the uniaxial ENZ-SPR phase-matching condition, which can be used for designing structures with tuned resonant frequencies and tailored geometries for different applications. As a proof of concept, we illustrated the refractive-index sensing in aqueous media, which can be exploited to detect various analytes, including those of biological interest. Upon comparing the sensing performance with structures built on Fe and Co substrates, we could readily observe the detrimental effect of losses. Because the designed structures with uniaxial ENZ metamaterials allow for high integrability and tunability of the working wavelength, we expect that this paper will stimulate development of plasmonic and magnetoplasmonic devices.

ACKNOWLEDGMENTS

This work was partially supported by the RNP, with resources from MCTIC, Grant No. 01250.075413/2018-04, under the Radiocommunication Reference Center (Centro de Referência em Radiocomunicações - CRR) project of the National Institute of Telecommunications (Instituto Nacional de Telecomunicações - Inatel), Brazil. The authors wish also acknowledge financial support from the Brazilian agencies FAPESP (2018/22214-6) and the National Council for Scientific and Technological Development-CNPq (429496/2018-4, 305958/2018-6).

[1] J. Chen, P. Albella, Z. Pirzadeh, P. Alonso-González, F. Huth, S. Bonetti, V. Bonanni, J. Åkerman, J. Nogués, P. Vavassori, A. Dmitriev, J. Aizpurua, and R. Hillenbrand, Small **7**, 2341 (2011).

[2] V. I. Belotelov, I. A. Akimov, M. Pohl, V. A. Kotov, S. Kasture, A. S. Vengurlekar, A. V. Gopal, D. R. Yakovlev, A. K. Zvezdin, and M. Bayer, Nat. Nanotech. **6**, 370 (2011).

[3] L. E. Kreilkamp, V. I. Belotelov, J. Y. Chin, S. Neutzner, D. Dregely, T. Wehlus, I. A. Akimov, M. Bayer, B. Stritzker, and H. Giessen, Phys. Rev. X **3**, 041019 (2013).

[4] A. R. Davoyan, A. M. Mahmoud, and N. Engheta, Opt. Exp. **21**, 3279 (2013).

[5] M. Moccia, G. Castaldi, V. Galdi, A. Alù, and N. Engheta, J. Phys. D: Appl. Phys. **47**, 025002 (2014).

[6] X. Luo, M. Zhou, J. Liu, T. Qiu, and Z. Yu, Appl. Phys. Lett. **108**, 131104 (2016).

[7] A. V. Kimel, A. Kirilyuk, P. A. Usachev, R. V. Pisarev, A. M. Balbashov, and T. Rasing, Nature **435**, 655 (2005).

[8] K. Vahaplar, A. M. Kalashnikova, A. V. Kimel, D. Hinzke, U. Nowak, R. Chantrell, A. Tsukamoto, A. Itoh, A. Kirilyuk, and Th. Rasing, Phys. Rev. Lett. **103**, 117201 (2009).

[9] A. Kirilyuk, A. V. Kimel, and T. Rasing, Rev. Mod. Phys. **82**, 2731 (2010).

[10] J. R. Mejía-Salazar and O. N. Oliveira, Jr, Chem. Rev. **118**, 10617 (2018).

[11] K. Kämpf, S. Kübler, F. W. Herberg, and A. Ehresmann, J. Appl. Phys. **112**, 034505 (2012).

[12] Y. Shoji, Y. Shirato, and T. Mizumoto, Jpn. J. Appl. Phys. **53**, 022202 (2014).

[13] B. Caballero, A. García-Martín, and J. C. Cuevas, ACS Photon. **3**, 203 (2016).

[14] A. Otto, Z. Phys. **216**, 398 (1968).

[15] E. Kretschmann and H. Raether, Z. Naturforsch **23a**, 2135 (1968).

[16] J. A. Girón-Sedas, F. Reyes Gómez, P. Albella, J. R. Mejía-Salazar, O. N. Oliveira, Jr., Phys. Rev. B **96**, 075415 (2017).

[17] E. Moncada-Villa, O. N. Oliveira, Jr., J. R. Mejía-Salazar, J. Phys. Chem. C **123**, 3790 (2019).

[18] D. Traviss, R. Bruck, B. Mills, M. Abb, and O. L. Muskens, Appl. Phys. Lett. **102**, 121112 (2013).

[19] V. G. Veselago, Sov. Phys. Usp. **10**, 509 (1968).

[20] J. B. Pendry, A. J. Holden, D. J. Robbins, and W. J. Stewart, IEEE Trans. Microwave Theory Tech. **47**, 2075 (1999).

[21] C. M. Soukoulis, S. Linden, and M. Wegener, Science **315**, 47 (2007).

[22] H. T. Nguyen, T. S. Bui, S. Yan, G. A. E. Vandenbosch, P. Lievens, L. D. Vu, and E. Janssens, Appl. Phys. Lett. **109**, 221902 (2016).

[23] R. A. Shelby, D. R. Smith, and S. Schultz, Science **292**, 77 (2001).

[24] A. Grbic and G. V. Eleftheriades, J. Appl. Phys. **92**, 5930 (2002).

[25] D. Schurig, J. J. Mock, and D. R. Smith, Appl. Phys. Lett. **88**, 041109 (2006).

[26] S. Zhang, W. J. Fan, B. K. Minhas, A. Frauenglass, K. J. Malloy, and S. R. J. Brueck, Phys. Rev. Lett. **94**, 037402 (2005).

[27] Q. Zhao, L. Kang, B. Du, H. Zhao, Q. Xie, X. Huang, B. Li, J. Zhou, and L. Li, Phys. Rev. Lett. **101**, 027402 (2008).

[28] L. V. Alekseyev, E. E. Narimanov, T. Tumkur, H. Li, Yu. A. Barnakov, and M. A. Noginov, Appl. Phys. Lett. **97**, 131107 (2010).

[29] A. Poddubny, I. Iorsh, P. Belov, and Y. Kivshar, Nat. Photonics **7**, 958 (2013).

[30] K. V. Sreekanth, Y. Alapan, M. ElKabbash, E. Ilker, M. Hinczewski, U. A. Gurkan, A. De Luca, and G. Strangi, Nat. Mater. **15**, 621 (2016).

[31] X. Chen, C. Zhang, F. Yang, G. Liang, Q. Li, and L. J. Guo, ACS Nano **11**, 9863 (2017).

[32] A. K. Zvezdin and V. A. Kotov, *Modern Magnetooptics and Magnetooptical Materials*, 1st ed. (Taylor and Francis, London, 1997).

[33] J. A. Girón-Sedas, J. R. Mejía-Salazar, E. Moncada-Villa, and N. Porras-Montenegro, Appl. Phys. Lett. **109**, 033106 (2016).

[34] O. Levy and D. Stroud, Phys. Rev. B **56**, 8035 (1997).

[35] B. Caballero, A. García-Martín, and J. C. Cuevas, Phys. Rev. B **85**, 245103 (2012).

[36] E. Ferreiro-Vila, J. B. González-Díaz, R. Fermento, M. U. González, A. García-Martín, J. M. García-Martín, A. Cebollada, G. Armelles, D. Meneses-Rodríguez, and E. M. Sandoval, Phys. Rev. B **80**, 125132 (2009).

[37] D. M. Whittaker and I. S. Culshaw, Phys. Rev. B **60**, 2610 (1999).

[38] K. Aslan, M. Weisenberg, E. Hortle, and C. D. Geddes, J. Appl. Phys. **106**, 014313 (2009).

[39] S. Shukla, N. K. Sharma, and V. Sajal, Braz. J. Phys. **46**, 288-293 (2016).

[40] L. Li, L. Sun, J. S. Gomez-Diaz, N. L. Hogan, P. Lu, F. Khatkhatay, W. Zhang, J. Jian, J. Huang, Q. Su, M. Fan, C. Jacob, J. Li, X. Zhang, Q. Jia, M. Sheldon, A. Alu, X. Li, and H. Wang, Nano Lett. **16**, 3936 (2016).

[41] J. Huang, X. Wang, X. L. Phuah, P. Lu, Z. Qi, and H. Wang, Mater. Today Nano **8**, 100052 (2019).

[42] R. L. Paldi, X. Sun, X. Wang, X. Zhang, and H. Wang, ACS Omega **5**, 2234 (2020).

[43] C. M. Miyazaki, F. M. Shimizu, J. R. Mejía-Salazar, O. N. Oliveira, Jr., and M. Ferreira, Nanotech. **28**, 145501 (2017).